

Intrinsic Up-Regulation of 2-AG Favors an Area Specific Neuronal Survival in Different In Vitro Models of Neuronal Damage

Sonja Kallendrusch^{1,2}, Constance Hobusch¹, Angela Ehrlich¹, Marcin Nowicki¹, Simone Ziebell³, Ingo Bechmann¹, Gerd Geisslinger³, Marco Koch¹, Faramarz Dehghani^{1,4*}

1 Institut für Anatomie, Universität Leipzig, Leipzig, Germany, **2** Lipid Signaling Forschungszentrum Frankfurt, Frankfurt, Germany, **3** Institut für Pharmakologie, Goethe Universität Frankfurt, Frankfurt, Germany, **4** Institut für Anatomie und Zellbiologie, Martin Luther Universität, Halle-Wittenberg, Halle, Germany

Abstract

Background: The endocannabinoid 2-arachidonoyl glycerol (2-AG) acts as a retrograde messenger and modulates synaptic signaling e. g. in the hippocampus. 2-AG also exerts neuroprotective effects under pathological situations. To better understand the mechanism beyond physiological signaling we used Organotypic Entorhino-Hippocampal Slice Cultures (OHSC) and investigated the temporal regulation of 2-AG in different cell subsets during excitotoxic lesion and dendritic lesion of long range projections in the entorhinal cortex (EC), dentate gyrus (DG) and the cornu ammonis region 1 (CA1).

Results: 2-AG levels were elevated 24 h after excitotoxic lesion in CA1 and DG (but not EC) and 24 h after perforant pathway transection (PPT) in the DG only. After PPT diacylglycerol lipase alpha (DAGL) protein, the synthesizing enzyme of 2-AG was decreased when *Dagl* mRNA expression and 2-AG levels were enhanced. In contrast to DAGL, the 2-AG hydrolyzing enzyme monoacylglycerol lipase (MAGL) showed no alterations in total protein and mRNA expression after PPT in OHSC. MAGL immunoreaction underwent a redistribution after PPT and excitotoxic lesion since MAGL IR disappeared in astrocytes of lesioned OHSC. DAGL and MAGL immunoreactions were not detectable in microglia at all investigated time points. Thus, induction of the neuroprotective endocannabinoid 2-AG might be generally accomplished by down-regulation of MAGL in astrocytes after neuronal lesions.

Conclusion: Increase in 2-AG levels during secondary neuronal damage reflects a general neuroprotective mechanism since it occurred independently in both different lesion models. This intrinsic up-regulation of 2-AG is synergistically controlled by DAGL and MAGL in neurons and astrocytes and thus represents a protective system for neurons that is involved in dendritic reorganisation.

Citation: Kallendrusch S, Hobusch C, Ehrlich A, Nowicki M, Ziebell S, et al. (2012) Intrinsic Up-Regulation of 2-AG Favors an Area Specific Neuronal Survival in Different In Vitro Models of Neuronal Damage. PLoS ONE 7(12): e51208. doi:10.1371/journal.pone.0051208

Editor: Pranela Rameshwar, University of Medicine and Dentistry of New Jersey, United States of America

Received: October 1, 2012; **Accepted:** October 30, 2012; **Published:** December 20, 2012

Copyright: © 2012 Kallendrusch et al. This is an open-access article distributed under the terms of the Creative Commons Attribution License, which permits unrestricted use, distribution, and reproduction in any medium, provided the original author and source are credited.

Funding: This study was supported by the BMBF project Tierversuchersatzmethoden and by the Lipid Signaling Forschungszentrum Frankfurt (LiFF). The funders had no role in study design, data collection and analysis, decision to publish, or preparation of the manuscript.

Competing Interests: The authors have declared that no competing interests exist.

* E-mail: Faramarz.Dehghani@medizin.uni-halle.de

Introduction

The endocannabinoid (eCB) system was shown to be involved in processes of neurodegeneration. Increased concentrations of eCBs such as 2-arachidonoylglycerol (2-AG) were found after different brain injuries [1] and various cannabinoids protected against ischemia, excitotoxicity or traumatic brain injury (TBI) [2,3,4,5]. Furthermore, the involvement of the eCB system in neurodegenerative diseases, like MS, Parkinson's, Huntington's and Alzheimer's disease is more and more unraveled [6,7,8,9].

Excitotoxic neuronal damage is reduced by 2-AG acting as a retrograde neurotransmitter decreasing neuronal firing at glutamatergic synapses [10]. Affecting different cannabinoid receptors and down-regulating the NFκB pathway 2-AG is involved in analgesia and anti-inflammatory processes [4,5,11,12,13]. The cannabinoid receptors type 1 (CB₁) and type 2 (CB₂) are the main molecular targets of 2-AG [14,15]. CB₁ is the most abundant G

protein-coupled receptor in the brain and resides at the pre-synaptic side of neuronal synapses [16], whereas CB₂ is mainly situated on immunoregulatory cells, like microglial cells [17,18]. There are several reports in the literature indicating further not yet cloned cannabinoid receptors that might be activated by 2-AG as well [5,19]. 2-AG is synthesized on demand from membrane glycerophospholipids by specific enzymes. Sn-1-diacylglycerol lipase alpha (DAGL) is the primary biosynthetic enzyme of 2-AG, found at the post-synapse of neurons [20]. Endocannabinoid signaling is further controlled by enzymatic hydrolysis and the principal 2-AG hydrolyzing enzyme is monoacylglycerol lipase (MAGL) being ascribed for 85% of total 2-AG break down [21,22].

However, so far little is known about the contribution of different glial cell populations to 2-AG regulation and the time course of its induction. Moreover, the precise regional control of 2-AG in different brain areas still remains unknown. Therefore, we

here compared the induction of the 2-AG regulatory machinery in an *in vitro* model of Organotypic Hippocampal Slice Cultures (OHSC) and investigated the temporal changes in 2-AG levels and its main enzymes DAGL and MAGL after 1) long-range projection damage as it occurs in stroke by transection of the perforant pathway and 2) excitotoxic lesion as a central mechanism of neuronal damage by application of NMDA. The excitotoxic lesions were performed with low (10 μ M) and high (50 μ M) NMDA doses to verify how sensitive the 2-AG machinery responds to an excitotoxic insult.

The perforant pathway connects two evolutionary distinct brain regions, namely the entorhinal cortex (EC) and the outer molecular layer of the dentate gyrus (DG) and its transection allows the study of cellular and inflammatory responses not only at the lesion site but also of anterograde projection areas [23,24,25,26,27]. In the model of excitotoxicity the vulnerability of different areas within the OHSC can be analyzed. The regulation of 2-AG levels and the main synthesizing and hydrolyzing enzymes were assessed up to 72 hours after perforant pathway transection (PPT) and excitotoxicity in OHSC. Moreover, the respective cell types being responsible for 2-AG metabolism, namely neurons, astrocytes or microglia were studied.

Materials and Methods

Ethics Statement

All animal experiments have been approved by the ethics committees of the German federal state of Saxonia and were performed in accordance with the Policy on Ethics and the Policy on the Use of Animals in Neuroscience Research as approved by the directive 2010/63/EU of the Council of the European Union on the protection of animals used for scientific purposes. Animals were maintained under a standard and a 12:12 hr light/dark schedule and constant temperature with food and water available *ad libitum* for the female rat. All efforts were made to minimize suffering.

Organotypic Hippocampal Slice Cultures (OHSC)

8-day old Wistar rats were used to prepare OHSC. After decapitation the brains were dissected under aseptic conditions and transferred to 4°C minimal essential medium (MEM; Gibco BRL Life Technologies, Eggenstein, Germany) containing 1% (v/v) glutamine (Gibco) (Stoppini et al. 1991). With a sliding vibratome (Leica VT 1200 S, Leica Microsystems AG, Wetzlar, Germany) brains were horizontally cut in 350 μ m-thick slices. After dissection of the hippocampus the slices were immediately placed on cell culture inserts (pore size 0.4 μ m; Millipore, Schwalbach/Ts., Germany) in 6-well culture dishes (Falcon, BD Biosciences Discovery Labware, Bedford, MA) containing 1 ml slice culture medium (50% (v/v) MEM, 25% (v/v) Hanks' balanced salt solution (HBSS, Gibco), 25% (v/v) normal horse serum (NHS, Gibco), 2% (v/v) glutamine, 1.2 mg/ml glucose (Braun, Melsungen, Germany), 0.1 mg/ml streptomycin (Sigma-Aldrich, Deisenhofen, Germany), 100 μ g/ml penicillin (Sigma-Aldrich), 0.8 μ g/ml ascorbic acid (Sigma-Aldrich) and 1 μ g/ml insulin (Boehringer, Mannheim, Germany), pH 7.4) per well. The slice cultures were kept at 35°C in a fully-humidified atmosphere with 5% (v/v) CO₂ for 6 days until lesion was set. The culture medium was changed every other day.

Primary cell culture

Primary cell cultures of microglial cells and astrocytes were isolated from cerebral cortices of neonatal Wistar rats (P1). The meninges were removed and the cerebral cortices were dissociated

in Ca²⁺/Mg²⁺-free HBSS, containing trypsin (4 mg/ml, Boehringer) and DNase (0.5 mg/ml, Worthington, Bedford, MA, USA). Tissue culture flasks (75 cm², Falcon) were beforehand coated with poly-L-lysine (Sigma-Aldrich) and contained cell culture media (DMEM (Gibco), 4.5 g/L glucose (Gibco), 10% (v/v) fetal bovine serum (FBS, Gibco), 1% (v/v) glutamine, 100 μ g/ml penicillin and 100 μ g/ml streptomycin) when cells were added and cultured until further use. Microglial cells were separated from the astrocytic monolayer and were subsequently plated into 24-well dishes coated with poly-L-lysine with cell culture medium containing 2% (v/v) FBS. Astrocyte cultures were also transferred one day prior to experiments into 24-well dishes coated with poly-L-lysine. Microglia and astrocytes were treated with 10 ng/ml lipopolysaccharide (LPS) for 4 hours (h).

For primary cultures of hippocampal neurons a modified method described by Brewer and colleagues was used [28]. Briefly, Wistar rats P0 were used and brains were dissected quickly. The meninges were removed and the brains were placed into an ice-cold HBSS solution. Subsequently the hippocampi were dissected and incubated in Neurobasal Medium (Gibco) containing BSA (Sigma-Aldrich) and papain (1 mg/ml, Sigma-Aldrich) for 20 min at 37°C. Neurons were isolated by dissociation and cultured onto poly-L-lysine-coated coverslips in 24-well dishes in Neurobasal medium supplemented with B-27 (Gibco), GlutaMAX (Gibco) and penicillin/streptomycin at 37°C in a humidified atmosphere with 5% (v/v) CO₂ for 2 weeks.

Excitotoxicity lesion

The OHSC were randomly divided into different treatment groups and were treated according to the following treatment protocol:

CTL: Unlesioned OHSC (n = 5) were kept in culture medium for 9 days *in vitro* (div) without any treatment and served as controls.

JZL184: Unlesioned OHSC (n = 6) were kept in culture medium until 6 div. At 6 div the culture medium was supplemented with 1 μ M JZL 184 until 9 div.

NMDA: OHSC were kept in culture medium for 6 days, lesioned with NMDA (50 μ M; n = 8, Sigma-Aldrich) for 4 hours and maintained in culture medium until 9 div.

NMDA+JZL184: OHSC were lesioned at 6 div with NMDA (50 μ M; n = 13, Sigma-Aldrich) for 4 h and kept in culture medium supplemented with JZL 184 (1 μ M) until 9 div.

OHSC treatment and 2-AG measurement. In an additional set of experiments OHSC were treated with low (10 μ M) or high (50 μ M) NMDA concentrations for 4 h and were further maintained in slice culture medium for 24 h or 72 h post lesion (hpl). Controls were cultured with slice culture medium until 4 h, 24 h and 72 h, simultaneously with the NMDA treated OHSC. At 4 h, 24 h and 72 h samples were collected and processed for immunohistochemistry or LC-MS/MS as described below.

Perforant Pathway Transection (PPT)

The PPT was mechanically set at 6 div by using a disposable ophthalmic scalpel with a stainless steel blade (Feather, Osaka, Japan). A binocular (Zeiss, Jena, Germany) was used to performed PPT within OHSC. The cut was set through the perforant pathway following the sulcus between the hippocampus and the EC [29]. Dissection of the EC, the DG and the cornu ammonis 1 (CA1) region was done 0, 1, 6, 12, 24, 48 or 72 hpl. Similar regions of three OHSC were pooled and shock frozen in liquid nitrogen. The tissues were stored at -80°C and processed not exceeding three days.

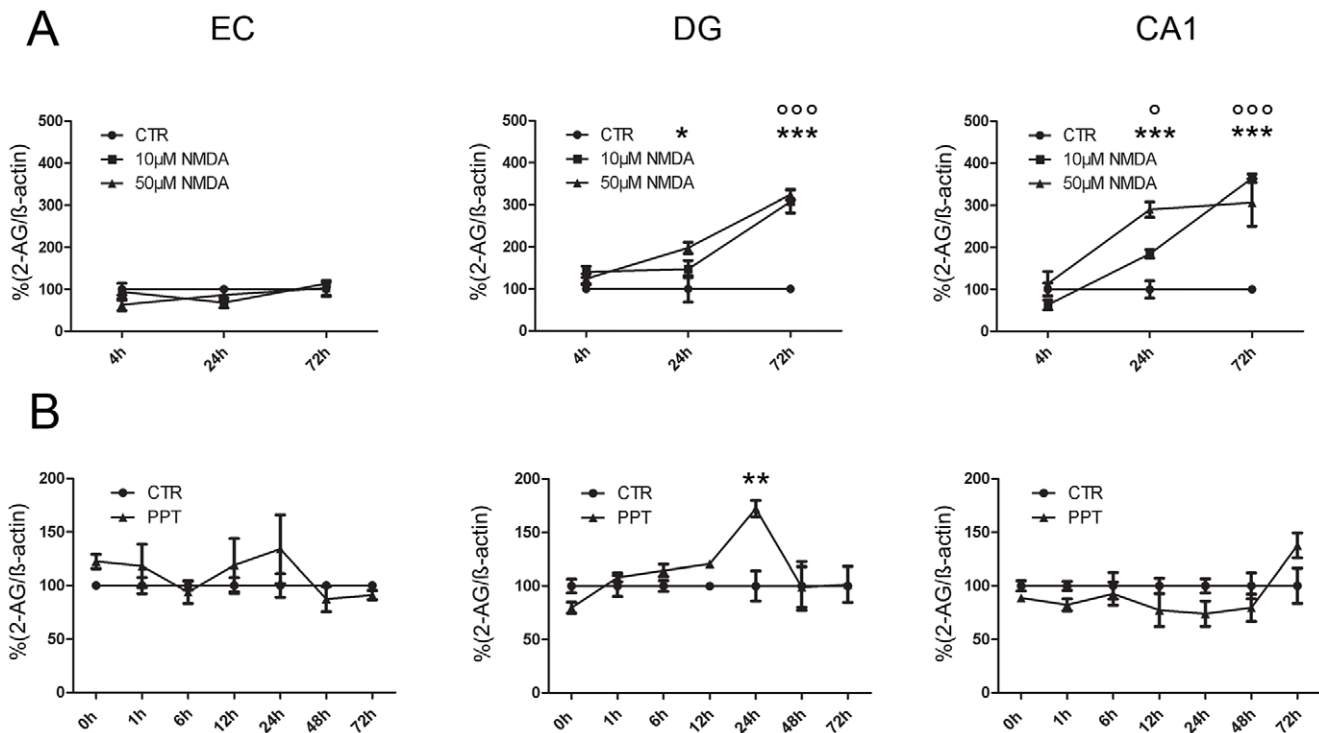


Figure 1. Intrinsic 2-AG regulation after neuronal damage - excitotoxic NMDA lesion and PPT. 2-AG levels in EC, DG and the CA1 region normalized against β -actin immunosignals. Control condition (CTR) of each time-point was set as 100% (black cycles). (A) 2-AG levels after application of 10 μ M and 50 μ M NMDA. In the DG an increase in 2-AG was seen 24 hpl after 50 μ M of NMDA. After 72 hpl 2-AG levels were elevated significantly independent of the NMDA concentration. In the CA1 region increased 2-AG levels were measured 24 and 72 hpl after 10 μ M and 50 μ M NMDA treatment (n = 3, °sig. for 10 μ M NMDA, *sig. for 50 μ M NMDA, °p < 0.05, °°° or ***p < 0.001). (B) 2-AG levels after PPT. In EC 2-AG levels (gray circles) did show a non significant alteration at 1 hpl in comparison to the respective CTR. In the DG, 2-AG was significantly increased 24 hpl (n = 4, **p < 0.01) and in the CA1 region 2-AG levels did not differ significantly from CTR values (p > 0.05). doi:10.1371/journal.pone.0051208.g001

LC-MS/MS

Sample Extraction. Lipid extraction has been carried out as previously described [30,31]. Briefly, 70 μ l ice cold H₂O was added to the sample prior to homogenation by a mixer mill 400 (Retsch, Haan, Germany) for 90 sec at 25 Hz. Next, from the homogenate 20 μ l was collected to determine the beta-actin content by Western Blot analysis (see below). The remaining 50 μ l of the homogenized tissue samples were then further processed together with 25 μ l internal standard (IS), 50 μ l ethylacetate/n-hexan and 50 μ l H₂O. After 3 min at 10,000 rpm the samples were centrifuged and the organic phase was collected, the extraction procedure was repeated twice. Under nitrogen the ethylacetate phases evaporated and the eCB were assimilated in 25 μ l acetonitril in glass vials. 10 μ l were injected into an LC-MS/MS system (API, 5000, AB SCIEX, California, USA). Quality standards were always extracted with the samples for accuracy.

Determination of endocannabinoid concentrations. 2-AG and 1-AG were analyzed from the reconstituted samples. Deuterated analytes 2-AG-d₅, 1-AG-d₅ were used as IS. Under gradient conditions using a Luna HST C18 (2) column (100 mm L x 2 mm ID, 2.5 μ m particle size; Phenomenex, Aschaffenburg, Germany) HPLC analysis was performed. An API 5000 triple quadrupole mass spectrometer with a Turbo V source (Applied Biosystems, Darmstadt, Germany) in the negative ion mode was used to perform MS and MS/MS. For 2-AG the precursor-to-product ion transitions m/z 377 → 303 was applied and m/z 382 → 303 for the deuterated 2-AG-d₅ and 1-AG-d₅ for the multiple reaction monitoring (MRM) with a dwell time of 70 msec

respectively. The Analyst software (version 1.4; Applied Biosystems) was used to evaluate concentrations of calibration standards, quality controls and samples. <15% over the range of calibration were accepted as intra-day and inter-day variations in accuracy.

Semi-quantitative real time PCR (rtPCR)

The site specific and time dependent changes in enzymes, DAGL and MAGL were analyzed by quantitative rtPCR. Tissue was harvested and stored in RTL_{later} (Qiagen) at -80°C until further use. Total RNA was extracted from the cells using TRIzol reagent (Invitrogen) according to the manufacturer's instructions. RNA was measured and controlled for its purity by the A260/280 ratio. Total RNA was immediately reversely transcribed (Superscript II, Invitrogen) with oligo(dT) primer cDNA. 50 ng of total RNA was subjected to rtPCR using Platinum-SYBR Green® qPCR Supermix (Invitrogen). Oligonucleotide primers (Tab. S1) were designed with the Primer3 software to flank intron sequences. All primers were synthesized by MWG Biotech (Eversberg, Germany) and diluted to 10 pmol/ μ l. Quantitative rtPCR was performed by an CFX9 (Bio Rad laboratories, München, Germany) using the following protocol: 3 min at 95°C and 40 cycles of 10 s at 95°C and 30 s at 61°C. A product melting curve was recorded to confirm the presence of a single amplicon. The correct amplicon size and identity were additionally confirmed by agarose gel electrophoresis. Standard curves with serial dilutions of cDNA were generated for each primer pair to assert linear amplification. Threshold cycle (C_t) values were set within the exponential phase of the PCR. After normalization to rodent

Table 1. Relative changes in 2-AG levels.

EC (NMDA)	2-AG (%)		DG (NMDA)	2-AG (%)		CA1 (NMDA)	2-AG (%)	
	10 μ M	50 μ M		10 μ M	50 μ M		10 μ M	50 μ M
4 hpl	94; p>0.05	63; p>0.05	4 hpl	140; p>0.05	124; p>0.05	4 hpl	63; p>0.05	114; p>0.05
24 hpl	68; p>0.05	87; p>0.05	24 hpl	147; p>0.05	198; p<0.01	24 hpl	185; p>0.05	290; p<0.001
72 hpl	114; p>0.05	103; p>0.05	72 hpl	308; p<0.001	324; p<0.001	72 hpl	364; p<0.001	307; p<0.001
EC (PPT)	2-AG (%)	DG (PPT)	2-AG (%)	CA1 (PPT)	2-AG (%)			
0 hpl	122; p>0.05	0 hpl	79; p>0.05	0 hpl	89; p>0.05			
1 hpl	118; p>0.05	1 hpl	107; p>0.05	1 hpl	82; p>0.05			
6 hpl	94; p>0.05	6 hpl	114; p>0.05	6 hpl	93; p>0.05			
12 hpl	119; p>0.05	12 hpl	120; p>0.05	12 hpl	77; p>0.05			
24 hpl	134; p>0.05	24 hpl	172; p<0.01	24 hpl	74; p>0.05			
48 hpl	87; p>0.05	48 hpl	98; p>0.05	48 hpl	80; p>0.05			
72 hpl	91; p>0.05	72 hpl	101; p>0.05	72 hpl	138; p>0.05			

doi:10.1371/journal.pone.0051208.t001

glyceraldehyde 3-phosphate dehydrogenase (GAPDH) primer, ΔC_t values were used to calculate the relative expression levels.

Western Blot analysis

Tissue was collected and immediately stored in lysis buffer at -80°C until further use. Protein was extracted in lysis buffer containing 80 mM Tris, 70 mM SDS, 0.3 M Saccharose, 3 mM sodium orthovanadate and 0.5 mM phenylmethylsulfonyl fluoride (PMSF) at pH 7.4. Five μg protein were loaded onto a 7.5% or 12.5% (w/v) sodium dodecylsulfate–polyacrylamide gel. Proteins were electrotransferred to nitrocellulose membranes and non-specific protein-binding sites were blocked for 1 h with 5% (w/v) milk (Carl Roth, Karlsruhe, Germany) or 5% (v/v) Roti-block solution (Carl Roth, Karlsruhe, Germany) in TBST. Primary antibodies were diluted in 5% (w/v) milk or 5% (v/v) Roti block in TBST and membranes were incubated over-night. The following primary antibodies were used: rabbit polyclonal antibody against human DAGL (diluted 1:2000, Frontier Science, cat.-no DGLA-Rb-Af380), rabbit polyclonal antibody against human MAGL (diluted 1:1000; developed by K. Mackie) and mouse monoclonal antibody directed against human beta-actin (diluted 1:40000; cat.-No A1978, Sigma-Aldrich). Membranes were washed and the secondary horse radish peroxidase-conjugated antibodies were applied for 1 h (anti-rabbit, 1:1000; cat.-No PI 1000, Vektor laboratories, Burlingame, CA; anti-mouse IgG, 1:4000; cat.-No CP01, Millipore, Billerica, USA). The signal of bound antibody was visualized by enhanced chemiluminescence (ECL detection system, Millipore) with radiographic films (Kodak, Stuttgart, Germany). ImageJ image analysis software (version 1.43, imagej.nih.gov/ij/download/) was used for semiquantification of the immunoreactive bands. Preabsorption with the corresponding blocking peptide was used to control the specificity of the MAGL antibody (Fig. S1A).

Immunohistochemistry

For 4 h OHSC were fixed in 4% (w/v) PFA, washed and incubated in 15% (w/v) sucrose before sectioning (14 μm) on a cryostat 3050 S (Leica, Wetzlar, Germany). After blocking unspecific bindings by normal goat serum (1:20 in PB saline (PBS)/Triton) for 30 min primary antibodies were added for 16 h in PBS/Triton containing 0.5% (w/v) bovine serum albumin: DAGL (diluted 1:200, Frontier Science, cat.-no DGLA-Rb-Af380), MAGL (diluted 1:200, Cayman Chemicals, cat no. 100035, Fig. S1B), Vglut1 (diluted 1:1000, synaptic systems, cat no. 135311), NeuN (diluted 1:200; cat.-No MAB377, Millipore), GFAP (diluted 1:200; cat. No 556330 BD Pharmingen) and biotinylated isolectin B₄ (IB₄) (diluted 1:50; cat.-No FL-1201 Vector Laboratories).

Triple-immunofluorescence staining was done using the primary antibodies against DAGL or MAGL combined with IB₄ and either with NeuN or GFAP respectively. Sections were washed in PBS prior to application of the secondary antibodies Alexa flour dye 568 (1:500, goat-anti rabbit IgG) and Alexa flour dye 633 (1:100, goat anti-mouse IgG; Invitrogen, Karlsruhe, Germany) for 1 h. The sections were coverslipped with Dako fluorescent mounting medium (Dako) and visualized by a Zeiss LSM 510 Meta confocal laser scanning system equipped with helium neon lasers (543 and 633 nm excitation lines) and an argon laser (488 nm excitation line).

Propidium Iodide (PI) labeling and confocal laserscanning microscopy

Two hours prior to fixation 5 $\mu\text{g}/\text{ml}$ PI was added to the slice culture medium. OHSC were then washed in PB and mounted

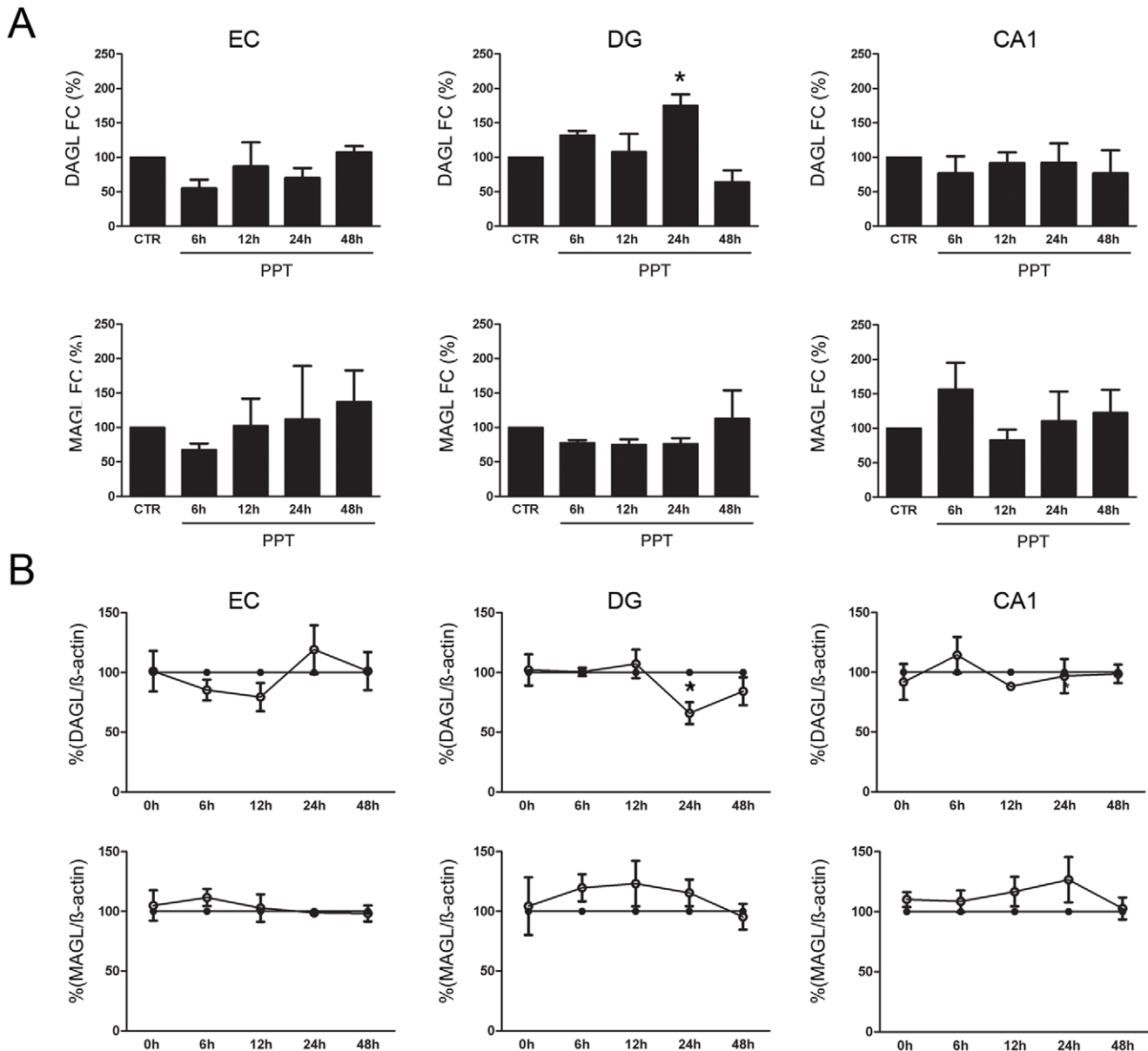


Figure 2. Enzymatic regulation of 2-AG after PPT. (A) *Dagl* and *Magl* mRNA regulation after PPT in the entorhinal cortex and the hippocampus after PPT. *Dagl* was increased after 24 hpl of PPT in the DG. (n = 3, *p < 0.05) (B) DAGL (open cycles) and MAGL (open cycles) protein regulation after PPT in the entorhinal cortex and the hippocampus after PPT. DAGL was decreased after 24 hpl of PPT in the DG compared to the respective control (closed cycles). (n = 3, *p < 0.05). doi:10.1371/journal.pone.0051208.g002

with DAKO fluorescent mounting medium (DAKO Diagnostika GmbH, Hamburg, Germany) and were analyzed with a Zeiss confocal laser scanning microscope using the helium neon laser 543 (LSM 510, Zeiss, Göttingen, Germany). With 160-fold magnification images were obtained using the Z-mode of the confocal microscope, optically cutting the OHSC in 2 μm-thick sections. Images were then converted into a binary image and Image J software (version 1.43, imagej.nih.gov/ij/download/) was used for PI-positive neuronal nuclei counting throughout the granule cell layer (GCL) of the dentate gyrus. To correct for inter experiment variances the different conditions were normalized to the respective NMDA condition.

siRNA transfection

MAGL gene silencing was carried out using siRNA (target sequence: 5'-CAGCGTGCTGTCTCGGAACAA-3'; sense strand: 5'-GCGUCUGUCUCGGAACAATT-3'; antisense strand: 5'-UUGUCCGAGACAGCAGCTG-3'; cat. no.: SI03067736, Qiagen, Hilden, Germany) and GeneSilencer siRNA transfection reagent (Genlantis-BioCat, Heidelberg, Germany) in a 6-well-culture plate. AllStars Negative Control siRNA (Qiagen) was used as a negative control. Transfection was performed according to manufacture's instructions at 5 div for 24 h before changing to native culture medium.

Table 2. Relative changes in protein and mRNA levels after PPT.

EC					
Protein (%)			mRNA (%)		
Group	DAGL	MAGL	Group	DAGL	MAGL
0 h	101, p>0.05	105, p>0.05	CTR	100, p>0.05	100, p>0.05
6 h	85, p>0.05	112, p>0.05	6 h	55, p>0.05	68, p>0.05
12 h	79, p>0.05	103, p>0.05	12 h	87, p>0.05	103, p>0.05
24 h	119, p>0.05	99, p>0.05	24 h	70, p>0.05	112, p>0.05
48 h	101, p>0.05	98, p>0.05	48 h	107, p>0.05	137, p>0.05
DG					
Protein (%)			mRNA (%)		
Group	DAGL	MAGL	Group	DAGL	MAGL
0 h	102, p>0.05	104, p>0.05	CTR	100, p>0.05	100, p>0.05
6 h	101, p>0.05	120, p>0.05	6 h	132, p>0.05	78, p>0.05
12 h	107, p>0.05	123, p>0.05	12 h	108, p>0.05	76, p>0.05
24 h	66, p<0.05	115, p>0.05	24 h	175, p<0.05	76, p>0.05
48 h	84, p>0.05	95, p>0.05	48 h	65, p>0.05	113, p>0.05
CA1					
Protein (%)			mRNA (%)		
Group	DAGL	MAGL	Group	DAGL	MAGL
0 h	92, p>0.05	110, p>0.05	CTR	100, p>0.05	100, p>0.05
6 h	114, p>0.05	109, p>0.05	6 h	77, p>0.05	157, p>0.05
12 h	88, p>0.05	117, p>0.05	12 h	92, p>0.05	83, p>0.05
24 h	97, p>0.05	130, p>0.05	24 h	92, p>0.05	111, p>0.05
48 h	99, p>0.05	103, p>0.05	48 h	77, p>0.05	123, p>0.05

doi:10.1371/journal.pone.0051208.t002

Statistical Analysis

Data from at least three independent experiments were expressed as mean values (+standard error of the mean (SEM) and statistically analyzed using one way ANOVA followed by Bonferroni posttests. Analysis was conducted with Graph Pad Prism software 5 (GraphPad software, La Jolla, USA) and p<0.05 was considered significant. Gene regulation was statistically evaluated by subjecting the $\Delta\Delta C_t$ values derived from each preparation samples to one way ANOVA.

Results

2-AG levels are up-regulated after excitotoxic lesion and PPT in areas of severe damage

Raw values of 3 pooled OHSC (EC, DG or CA1) contained about 3–5 ng/ml 2-AG under control conditions. The obtained 2-AG values were corrected for their β -actin content and were then given in percent values of the respective controls. The NMDA and PPT data was expressed in relation to their time controls, respectively (Fig. 1).

Excitotoxic lesion. Excitotoxic NMDA lesion and dendritic denervation led to an intrinsic up-regulation of 2-AG levels in specific brain regions, namely the DG and the CA1 region after excitotoxic lesion with low and high NMDA doses (NMDA, 10 μ M, 50 μ M, Fig. 1A). In the EC 2-AG levels remained at control levels after excitotoxic lesion with 10 μ M and 50 μ M NMDA until 72 hpl (Fig. 1A). In the DG 10 μ M NMDA

increased 2-AG levels 72 hpl (307.50%; p<0.001) but not at 4 hpl and 24 hpl (Fig. 1A). 50 μ M NMDA increased 2-AG levels at 24 hpl (197.60%) and 72 hpl (323.90%; p<0.001, Fig. 1A). 2-AG levels of the CA1 region treated with 10 μ M NMDA showed a significant increase at 24 hpl (184.70%; p<0.05) and 72 hpl (364.30%; p<0.001, Fig. 1A). After treatment with 50 μ M NMDA 2-AG was enhanced at 24 hpl (290.20%; p<0.001) and 72 hpl (306.70%; p<0.001, Fig. 1A). Single values of each group are presented in Table 1.

Perforant Pathway Transection (PPT). After PPT no significant changes of 2-AG levels were observed in the EC an CA1 region (Fig. 1B). In the DG 24 hpl 2-AG levels were significantly increased compared to controls (24 hpl, 172.20%; p<0.01, Fig. 1B). Thereafter 2-AG levels declined to control levels (Fig. 1B). Single values of each group are presented in Table 1.

Transcriptional dynamics of *Dagl* and *Magl* after PPT

Semi-quantitative real time PCR was used to investigate the intrinsic regulation of (*Dagl*) and (*Magl*) enzymes of 2-AG in the different regions over time.

In the EC and CA1 regions no changes of both mRNAs were observed after PPT. *Dagl* and *Magl* expression were not significantly different compared to the control OHSC (Fig. 2A). In the DG *Dagl* expression was significantly enhanced 24 hours after PPT (24 hpl, 175.40%; p<0.05, Fig. 2A) related to the respective controls. *Magl* expression did not show significant changes (Fig. 2A

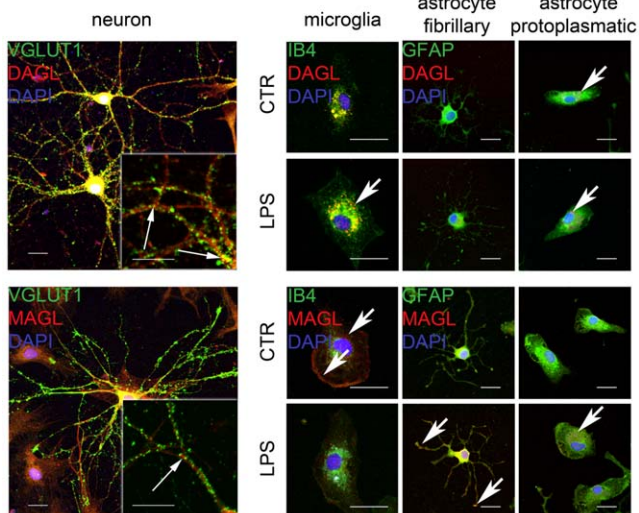


Figure 3. Immunocytochemical analyses of DAGL and MAGL in primary neuronal (left column), microglial (middle column) and astrocyte (left columns) cell cultures. In neurons, DAGL was distributed in the perikarya and in neuronal processes. VGLUT1 was co-localized with DAGL suggesting a close surveillance of glutamate by DAGL (arrows). MAGL was distributed in primary neuronal cultures but displayed no overlap with VGLUT1 (arrow). **Microglial cells** were labeled with DAGL in their cell bodies after LPS treatment. DAGL expression was stronger than in controls (arrow), whereas, MAGL expression in microglia was clearly visualized under control condition around the nucleus and at the outer edges (arrows) of the cells the labeling disappeared under LPS treatment (arrow). **Astrocytes** were not found immunoreactive for DAGL in fibrillary astrocytes under control condition, however DAGL was weakly induced after LPS treatment. Protoplasmic astrocytes displayed a robust DAGL immunoreaction in controls and after LPS stimulation as visualized in droplets throughout the cell body (arrows). MAGL was induced in both fibrillary and protoplasmic astrocytes after LPS treatment (arrows). Bar = 20 μ m. doi:10.1371/journal.pone.0051208.g003

Dynamics in DAGL and MAGL protein amount after PPT

Western Blot analysis was used to investigate the intrinsic regulation of DAGL and MAGL in different regions over time. The respective time controls were set to 100%. No changes in DAGL and MAGL were observed in the EC and CA1 regions after PPT as compared to the time control OHSC (Fig. 2B). After 24 hpl DAGL protein was significantly decreased in the DG after PPT (Fig. 2B, 24 hpl, 65.90%; $p < 0.05$) related to the respective controls. MAGL expression in the DG did not show significant changes (Fig. 2B). Single values of each group are presented in Table 2.

Cellular distribution of DAGL and MAGL in primary neurons, microglia and astrocyte cultures

In isolated primary neuronal cultures DAGL immunoreaction (IR) was observed within neuronal perikarya and processes. The double staining of DAGL and VGLUT1 showed punctual colocalizations (Fig. 3). MAGL IR was not observed to be co-localized with VGLUT1 in primary neuronal culture.

In primary microglia cultures DAGL IR was located in the cell body and became more intense after LPS treatment (Fig. 3). DAGL IR was differentially distributed in astrocyte subtypes: whereas fibrillary astrocytes showed a very weak DAGL IR after LPS treatment only, protoplasmic astrocytes displayed a few punctual immunoreactions spread throughout the cell body under both, control and LPS treated conditions (Fig. 3). In IB₄ positive

microglia, MAGL IR was found in the cytoplasm and at the cell borders. Interestingly MAGL IR was very weak after LPS treatment (Fig. 3). Fibrillary astrocytes displayed MAGL IR within their cell bodies. In LPS treated cells, MAGL IR was seen in the cell bodies and to a minor extent in their processes. The IR of MAGL in protoplasmic astrocytes was very weak, no alteration was observed between the control and the LPS treated condition.

Distribution of DAGL and MAGL in OHSC

Localizations of DAGL and MAGL IR were investigated by immunohistochemical staining with NEUN, GFAP and IB₄ in sections obtained from OHSC at 1 hpl, 6 hpl, 12 hpl and 24 hpl.

Perforant pathway transaction. DAGL IR was found in the cytoplasm of NeuN positive cells in control OHSC and in OHSC after PPT. Co-localization of DAGL IR with GFAP IR in astrocytes and IB₄ positive microglial cells was hardly detectable in control OHSC and no change was found in OHSC after PPT until 12 hpl (not shown). After 24 hpl the DAGL IR remained in the cytoplasm of neurons and a weak DAGL IR was seen in astrocytes. Reorganization of DAGL IR was also observed 24 hpl, the tight organization of the granular cell layer dispersed and DAGL IR was found in the outer third but vanished in the inner half of the granular layer (Fig. 4). In the hilus region of some PPT lesioned OHSC enhanced DAGL IR was seen, however this finding was not consistent in all PPT lesioned OHSC.

MAGL IR showed a punctual distribution in NeuN positive cells (Fig. 4). GFAP positive astrocytes showed a strong colocalization with the MAGL IR under control conditions. Microglial cells displayed only weak or no MAGL IR in OHSC (Fig. 4). Over time, microglial cells did not show a change of MAGL IR in OHSC. At 24 hpl (PPT) MAGL IR was lower in GFAP positive cells, no other changes in cellular distribution were observed over time (Fig. 4).

Excitotoxic lesion. DAGL IR was found in the cytoplasm of NeuN in OHSC after excitotoxic NMDA lesion and disappeared 24 hpl. After NMDA lesion DAGL IR was mainly found in astrocytes and no longer in neuronal cytoplasm (Fig. 4).

MAGL IR was located in GFAP positive astrocytes under control conditions and could not be seen after 24 hpl (NMDA) in GFAP positive cells (Fig. 4).

Intrinsic up-regulation of 2-AG after MAGL inhibition by JZL184 in OHSC

After JZL184 (1 μ M) application for 4 h 2-AG levels increased up to 35–45 ng/ml in OHSC and were significantly elevated in all investigated regions (EC, 736%; $p < 0.01$; DG, 688%; $p < 0.01$, CA1, 570%; $p < 0.05$, Fig. 5A).

Inhibition of MAGL by JZL184 and Magl knock-down using siRNA exerted neuroprotective effects after excitotoxic lesion

Non-lesioned control OHSC exhibited a good neuronal preservation with almost no PI positive neuronal nuclei. All conditions were normalized against NMDA and given in percent values (Fig. 5B). The application of 1 μ M JZL184 did not lead to any significant alterations within the number of PI positive neuronal nuclei as compared to CTR (JZL184, 0.24%, $p > 0.05$). Treatment of OHSC with 50 μ M NMDA for 4 hours at 6 div strongly increased the numbers of PI positive neuronal nuclei (NMDA, 100%, $p < 0.001$ vs. negative CTL) as compared to CTR. Application of 1 μ M JZL184 to NMDA-lesioned OHSC led to a significant reduction of PI positive neuronal nuclei as compared to

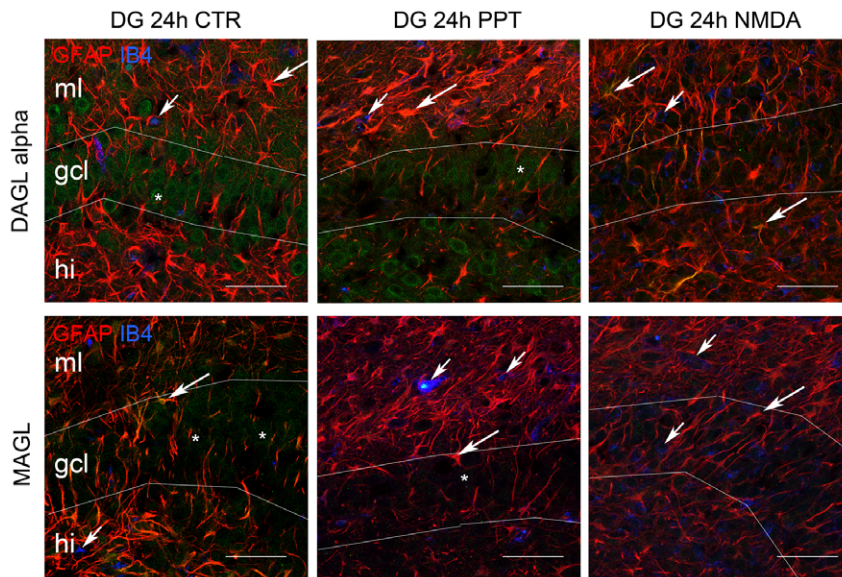


Figure 4. DAGL α and MAGL immunoreaction in OHSC 24 h after PPT. Images show the molecular layer (ml), the granular cell layer (gcl) and part of the hilus (hi) region. The enzymes DAGL and MAGL are given in green, GFAP in red and IB₄ positive microglial cells are displayed in blue. The asterisks indicate NeuN co-localized DAGL and MAGL staining in the gcl (NeuN data not shown). DAGL was co-localized with GFAP positive cells only after PPT and NMDA excitotoxic lesion but not in control OHSC (big arrows). IB₄ positive microglial cells were not DAGL immunoreactive under control conditions or after neuronal damage (small arrows). After PPT the DAGL was seen in the outer half of the gcl whereas the inner half of the granular cell layer was not labeled (24 hpl, asterisk). GFAP positive cells expressed a strong co-localization with the MAGL protein in control OHSC that disappeared 24 h after PPT and in NMDA lesioned OHSC (big arrows). A weak MAGL immunoreaction was found in vesicular structures in microglial cells presumably representing phagocytosis bodies in their cytoplasm (small arrows). (Bar = 50 μ m). doi:10.1371/journal.pone.0051208.g004

positive OHSC treated with NMDA alone (NMDA+1 μ M JZL184, 50.97%; $p < 0.05$ vs. NMDA, Fig. 5B).

Non-lesioned OHSC treated with negRNA or siRNA (negRNA, 0.28% siRNA, 0.28%) exhibited no different neuronal preservation as compared to control OHSC with almost no PI positive neuronal nuclei (CTL, 0.26%) in the DG. Treatment of OHSC with 50 μ M NMDA for 4 hours at 6 div strongly induced the numbers of PI positive neuronal nuclei (NMDA, 100%, $p < 0.001$ vs. CTL) as compared to untreated CTL. Application of negRNA to NMDA-lesioned OHSC showed no changes (NMDA+negRNA, 121.83%; $p > 0.05$ vs. NMDA), but the application of siRNA led to a significant reduction of PI positive neuronal nuclei compared to OHSC treated with NMDA alone (NMDA+siRNA, 33.45%; $p < 0.05$ vs. NMDA, Fig. 5C).

Discussion

Primary neurological insults are worsened by secondary accumulation of harmful mediators leading to delayed tissue damage and finally to persistent clinical and social disabilities for patients [32]. Therefore, one aim in current neuroscience research is the identification of biological mechanisms by which the protective properties of intrinsic brain mechanisms can be amplified with the final goal to develop clinical tools against secondary neuronal damage. 2-AG is commonly accepted as a beneficial mediator and an important member of the eCB system, well known to protect neurons after neuronal insults mainly by retrograde signaling finally leading to decreased neuronal excitation [4,33,34,35]. Since the cell-type specific and temporal regulation of 2-AG during secondary neuronal damage in the brain was still fragmentary, we chose two different neuronal lesion models to investigate whether the different areas within the hippocampal formation would respond with a distinct time

dependent and area specific 2-AG up-regulation after low and high concentrations of NMDA or PPT.

The EC showed no detectable changes in 2-AG levels after low or high NMDA concentrations. The DG however showed enhanced 2-AG levels 24 hours after the lesion with high NMDA concentrations. Interestingly, low NMDA doses were sufficient to enhance 2-AG significantly in the CA1 region. Being the region with the highest density of NMDA receptors the CA1 region is the most sensitive region to excitotoxic lesion [36]. Evidence exists that the density of the 2-AG hydrolyzing enzyme, MAGL, is low on the axon terminals of mossy cells and DAGL, the 2-AG synthesizing enzyme, was shown to be abundant at the Schaffer collateral CA1 region of the hippocampal formation [37,38,39]. This strengthens the relevance of 2-AG in the CA1 region during neuronal stress. Enhanced 2-AG response to low NMDA concentrations might be a possible mechanism to counteract the insult in the more susceptible CA1 region. Stimulation of the Schaffer collateral synapses shown by Stella et al. led also to an endogenous 2-AG release in rat OHSC [40] and also short-term synaptic depression was consistently enhanced by genetic inhibition of MAGL [41,42] supporting the present data.

CNS pathologies like stroke involve lesion of long range projections and a wide range of temporal cellular reorganization. We focused on intrinsic 2-AG regulation after a model of long range projection damage, the perforant pathway transection in OHSC. This model was described in detail recently [31] allowing clear differentiation of anterograde (DG), retrograde (EC) and more distant area (CA1) changes induced by axonal injury of long range projections without leading to neuronal cell death. At the direct axonal lesion site no changes of 2-AG were observed. However, at the site of anterograde (dendritic) lesion a maximum peak was seen 24 hours post lesion. We could clearly show that axonal degeneration resulted in a moderate 2-AG increase at the

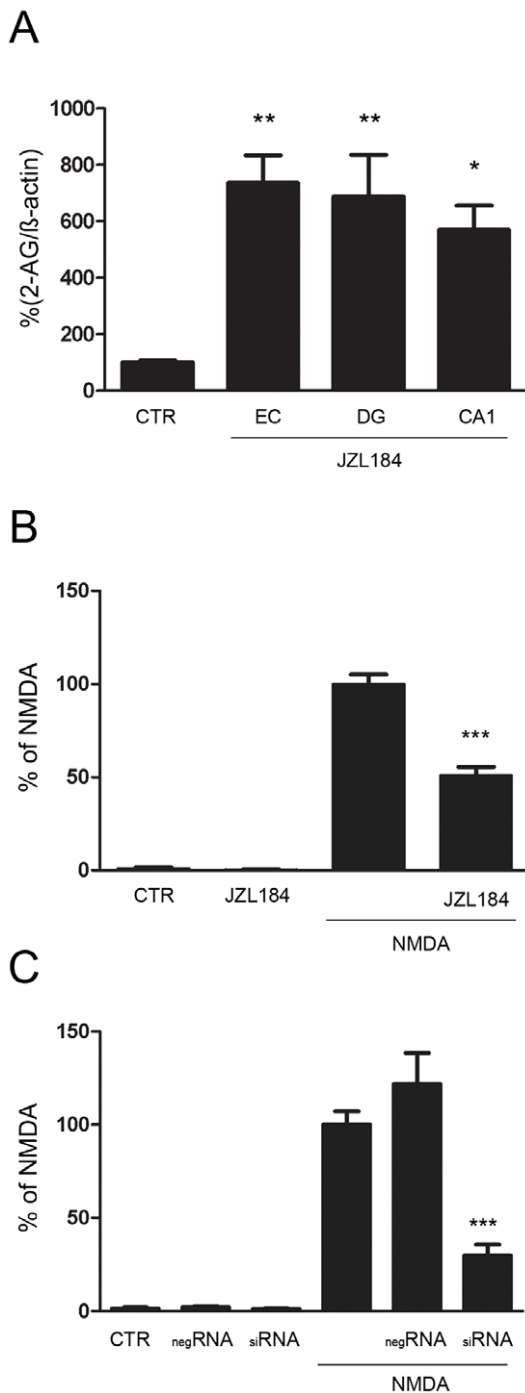


Figure 5. Inhibition of MAGL by JZL184 and siRNA exerted neuroprotective effects. (A) OHSC were treated for 4 h with JZL184 (1 μ M) at 6 div. 2-AG levels were significantly elevated in all investigated (EC, DG, CA1) regions compared to the respective control regions of untreated OHSC. (B) Decreased neuronal cell death was seen in excitotoxically lesioned OHSC treated with JZL184 compared to lesioned OHSC treated with NMDA alone. (C) MAGL knock down by siRNA reduced the number of degenerating neurons after NMDA-lesion. ($n > 3$, * = $p < 0.05$, ** = $p < 0.01$, *** = $p < 0.001$). doi:10.1371/journal.pone.0051208.g005

target area and had no further effects on 2-AG regulation in the CA1 region, postulating the involvement of 2-AG regulation in dendritic re-organisation.

To assess the involvement of 2-AG in dendritic reorganization we investigated the regulation of the main synthesizing (DAGL) and hydrolyzing (MAGL) enzymes of 2-AG. *Dagl* mRNA remained unchanged after PPT in the EC and was increased 24 hpl in the DG, whereas *Magl* mRNA remained at control levels. *DAGL*^{-/-} mice show reduced 2-AG levels and it was found that DAGL is functionally involved in neurogenesis [43,44]. Increased *Dagl* mRNA levels might therefore explain the enhanced 2-AG levels of the anterograde lesion site as suggested by a previous spinal cord study [45]. In our study the investigation of DAGL protein levels over time surprisingly revealed a decreased DAGL protein expression 24 hours after PPT.

A possible explanation for enhanced *Dagl* mRNA expression and increased 2-AG levels together with decreased DAGL protein expression might be ubiquitination of DAGL as reported in development and axonal growth [20,49]. Ubiquitination is common among proteins involved in signaling events, where rapid regulation is important. Very recently two enzymes (Phospholipase D1, Cyclooxygenase-1 (COX-1)) involved in arachidonic acid regulation were shown to be ubiquitinated [46,47]. Intra-cellular calcium concentration was responsible in human embryonic kidney 293 cells for ubiquitinated COX-1 degradation [46]. The fast turnover of proteins via the ubiquitin-proteasome system is a fundamental mechanism for cells to control signal transduction, cell cycle regulation and transcription [48,49]. Another hypothesis might be the reflectory increase in *Dagl* mRNA in response to decreased DAGL protein levels. To evaluate this hypothesis additional time points of investigation between 12 hpl and 24 hpl will be needed.

To clarify the regulation of DAGL and MAGL more precisely, we investigated their cellular distribution in neurons, microglia and astrocytes under control and LPS-stimulated conditions in OHSC as well as in primary cell cultures. DAGL was strongly found in neurons and was only weakly present in astrocytes of control OHSC. In primary neuronal cultures we found DAGL colocalized with Vglut1 at pre-synapses confirming previous reports in cerebellar, hippocampal and striatal neurons showing DAGL at the dendritic spines in the CA1 subfield, linked to the intracellular surface of the plasma membrane [38,39,50,51]. In the present study, we found a re-organization of DAGL immunoreaction especially after PPT towards the area of dendritic reorganization. Interestingly, the DAGL immunoreaction increased in astrocytes after both, PPT and excitotoxicity. Reactive GFAP positive astrocytes have been found to produce 2-AG and express DAGL in a valuable amount [52] either in vitro or in vivo in the epicenter of spinal cord injury [45]. In addition, our findings are in line with a previous descriptions of intense 2-AG production after stimulating isolated astrocytes with high ATP concentrations [53].

Microglia however did not show DAGL immunoreaction in OHSC, but in primary microglia culture. Interestingly, DAGL immunoreactivity was not observed in microglia after spinal cord injury [45], although microglia have been shown to produce important amounts of 2-AG in vitro [54,55].

The distribution of the degrading enzyme MAGL displayed a surprising pattern. Most studies focused on neuronal expression of MAGL, however the cellular expression of MAGL during NMDA lesion and PPT showed a low MAGL expression in astrocytes compared to controls by immunohistochemistry. It has previously been reported that astrocytes express the degrading enzyme MAGL [56,57]. Here, a clear MAGL immunoreaction in microglia was not found in OHSC but in microglial primary cell cultures. Recent studies suggest that the ABHD12 enzyme, highly expressed in microglia accounts for approx. 9% of total brain 2-

AG hydrolysis [58]. ABHD12 was suggested as adequate MAGL analogue for microglia as well as in related cell types of peripheral tissues [59]. The different distribution of DAGL and MAGL immunoreactivities in different cellular states suggests a highly defined expression pattern depending on the activation state of the cells. Therefore, our findings imply a qualitatively different contribution of 2-AG signaling to distinct lesion models as described for specific synapses and microcircuits.

CB₁ and DAGL are evolutionary closely associated, stating 2-AG as the endogenous ligand for CB₁ [10,60]. Interestingly, we observed no alteration in the amount of CB₁ protein in the DG 24 hpl, the primary target of 2-AG [31]. Recent reports found a decrease in CB₁ by internalization or downregulation after prolonged 2-AG stimulation in coronal brain section by [³⁵S] GTPγS binding [61]. The absence of MAGL led to compensatory desensitization of the CB₁ receptor in the brain as CB₁ receptor density and functional responses were attenuated [61]. Here, we used JZL184 to induce an up-regulation of intrinsic 2-AG levels and observed increased 2-AG levels in all investigated regions. It is reported that chronic inactivation of MAGL by JZL184 dramatically reduced 2-AG break-down, that led to a 10-fold increase of 2-AG levels in the brain as also shown in the present study [58,62]. However, JZL184 was less potent in the CA1 region than in the DG or the EC, supporting the lower occurrence of MAGL in the CA1 region.

To further demonstrate that intrinsic up-regulation of 2-AG, clearly accounts for neuronal protection, we treated NMDA lesioned OHSC with either JZL184 or MAGL siRNA and observed decreased neuronal damage in the granular cell layer of the dentate gyrus under both conditions. Other studies reported neuroprotective properties of 2-AG in neuronal excitotoxic models and other cellular settings by using exogenous 2-AG [11,63]. However, in vivo models of closed head injury and focal ischemia in mice elevated 2-AG levels were found after the lesion [4,64]. The early onset of 2-AG level up-regulation might be provoked by the blood-brain barrier (BBB) disruption as 2-AG levels were

shown to reduce BBB permeability 1–4 hours after brain injury [64,65].

In summary, 2-AG is intrinsically involved in general secondary damage regulation and strongly responds to excitotoxic and axonal damage in OHSC as a neuroprotective mediator. Furthermore the DAGL and MAGL dependent regulation of 2-AG is a dynamic interplay mainly of astrocytes and neurons embedded in time and cellular organization and involved in dendritic reorganisation.

Supporting Information

Table S1 Sequences of the used primers.

(TIF)

Figure S1 Specificity test for antibodies against MAGL by Western blot analyses.

(A) The antibody against MAGL showed two immunoreactive bands of about 35 kDa (1). Both bands were blocked by use of the respective blocking peptide (2). (B) MAGL fluorescent staining and MAGL fluorescent staining after preincubation with the respective peptide for 1 h. Bar = 50 μm.

(TIF)

Acknowledgments

The authors are deeply thankful to Dr. Helmut Schmidt (deceased in 2009) for his continuous support in the analysis of endocannabinoids by the LC/MS-MS method. Authors would like to thank H.-W. Korf, K. Mackie and W. Härtig for support.

Author Contributions

Conceived and designed the experiments: SK GG MK FD. Performed the experiments: SK AE CH. Analyzed the data: SK MK FD. Contributed reagents/materials/analysis tools: GG MN IB SZ. Wrote the paper: SK MK FD.

References

- Piomelli D (2003) The molecular logic of endocannabinoid signalling. *Nat Rev Neurosci* 4: 873–884.
- Nagayama T, Sinor AD, Simon RP, Chen J, Graham SH, et al. (1999) Cannabinoids and neuroprotection in global and focal cerebral ischemia and in neuronal cultures. *J Neurosci* 19: 2987–2995.
- van der Stelt M, Veldhuis WB, Bar PR, Veldink GA, Vliegthart JF, et al. (2001) Neuroprotection by Delta9-tetrahydrocannabinol, the main active compound in marijuana, against ouabain-induced in vivo excitotoxicity. *J Neurosci* 21: 6475–6479.
- Panikashvili D, Simeonidou C, Ben-Shabat S, Hanus L, Breuer A, et al. (2001) An endogenous cannabinoid (2-AG) is neuroprotective after brain injury. *Nature* 413: 527–531.
- Kreutz S, Koch M, Ghadban C, Korf HW, Dehghani F (2007) Cannabinoids and neuronal damage: differential effects of THC, AEA and 2-AG on activated microglial cells and degenerating neurons in excitotoxically lesioned rat organotypic hippocampal slice cultures. *Exp Neurol* 203: 246–257.
- Pisani V, Madoe G, Tassone A, Sciamanna G, Maccarrone M, et al. (2011) Homeostatic changes of the endocannabinoid system in Parkinson's disease. *Mov Disord* 26: 216–222.
- Casteels C, Vandeputte C, Rangarajan JR, Dresselaers T, Riess O, et al. (2011) Metabolic and type 1 cannabinoid receptor imaging of a transgenic rat model in the early phase of Huntington disease. *Exp Neurol* 229: 440–449.
- Zajicek JP, Apostu VI (2011) Role of cannabinoids in multiple sclerosis. *CNS Drugs* 25: 187–201.
- Mulder J, Zilberter M, Pasquare SJ, Alpar A, Schulte G, et al. (2011) Molecular reorganization of endocannabinoid signalling in Alzheimer's disease. *Brain* 134: 1041–1060.
- Katona I, Freund TF (2008) Endocannabinoid signaling as a synaptic circuit breaker in neurological disease. *Nat Med* 14: 923–930.
- Koch M, Kreutz S, Bottger C, Benz A, Maronde E, et al. (2011) Palmitoylethanolamide protects dentate gyrus granule cells via peroxisome proliferator-activated receptor-alpha. *Neurotox Res* 19: 330–340.
- Panikashvili D, Mechoulam R, Beni SM, Alexandrovich A, Shohami E (2005) CB1 cannabinoid receptors are involved in neuroprotection via NF-kappa B inhibition. *J Cereb Blood Flow Metab* 25: 477–484.
- Katona I, Urban GM, Wallace M, Ledent C, Jung KM, et al. (2006) Molecular composition of the endocannabinoid system at glutamatergic synapses. *Journal of Neuroscience* 26: 5628–5637.
- Howlett AC, Barth F, Bonner TI, Cabral G, Casellas P, et al. (2002) International Union of Pharmacology. XXVII. Classification of cannabinoid receptors. *Pharmacol Rev* 54: 161–202.
- Sugiura T, Kondo S, Sukagawa A, Nakane S, Shinoda A, et al. (1995) 2-Arachidonoylglycerol: a possible endogenous cannabinoid receptor ligand in brain. *Biochem Biophys Res Commun* 215: 89–97.
- Freund TF, Katona I, Piomelli D (2003) Role of endogenous cannabinoids in synaptic signaling. *Physiol Rev* 83: 1017–1066.
- Dittel BN (2008) Direct suppression of autoreactive lymphocytes in the central nervous system via the CB2 receptor. *Br J Pharmacol* 153: 271–276.
- Maresz K, Pryce G, Ponomarev ED, Marsicano G, Croxford JL, et al. (2007) Direct suppression of CNS autoimmune inflammation via the cannabinoid receptor CB1 on neurons and CB2 on autoreactive T cells. *Nat Med* 13: 492–497.
- Pertwee RG, Howlett AC, Abood ME, Alexander SP, Di Marzo V, et al. (2010) International Union of Basic and Clinical Pharmacology. LXXIX. Cannabinoid receptors and their ligands: beyond CB and CB. *Pharmacol Rev* 62: 588–631.
- Bisogno T, Howell F, Williams G, Minassi A, Cascio MG, et al. (2003) Cloning of the first sn1-DAG lipases points to the spatial and temporal regulation of endocannabinoid signaling in the brain. *J Cell Biol* 163: 463–468.
- Dinh TP, Carpenter D, Leslie FM, Freund TF, Katona I, et al. (2002) Brain monoglyceride lipase participating in endocannabinoid inactivation. *Proc Natl Acad Sci U S A* 99: 10819–10824.
- Blankman JL, Simon GM, Cravatt BF (2007) A comprehensive profile of brain enzymes that hydrolyze the endocannabinoid 2-arachidonoylglycerol. *Chem Biol* 14: 1347–1356.

23. Deller T (1997) The anatomy of the rat fascia dentata—new vistas. *Ann Anat* 179: 501–504.
24. Frotscher M, Heimrich B, Deller T (1997) Sprouting in the hippocampus is layer-specific. *Trends Neurosci* 20: 218–223.
25. Kovac AD, Kwidzinski E, Heimrich B, Bittigau P, Deller T, et al. (2004) Entorhinal cortex lesion in the mouse induces transsynaptic death of perforant path target neurons. *Brain Pathol* 14: 249–257.
26. Stoppini L, Buchs PA, Muller D (1991) A simple method for organotypic cultures of nervous tissue. *J Neurosci Methods* 37: 173–182.
27. Ramirez JJ (2001) The role of axonal sprouting in functional reorganization after CNS injury: lessons from the hippocampal formation. *Restor Neurol Neurosci* 19: 237–262.
28. Brewer GJ, Torricelli JR, Evege EK, Price PJ (1993) Optimized survival of hippocampal neurons in B27-supplemented Neurobasal, a new serum-free medium combination. *J Neurosci Res* 35: 567–576.
29. Del Turco D, Deller T (2007) Organotypic entorhino-hippocampal slice cultures—a tool to study the molecular and cellular regulation of axonal regeneration and collateral sprouting in vitro. *Methods Mol Biol* 399: 55–66.
30. Bishay P, Schmidt H, Marian C, Haussler A, Wijnvoord N, et al. (2010) R-flurbiprofen reduces neuropathic pain in rodents by restoring endogenous cannabinoids. *PLoS One* 5: e10628.
31. Kallendrusch S, Hobusch C, Ehrlich A, Ziebell S, Ueda N, et al. (2012) Site-specific and time-dependent activation of the endocannabinoid system after transection of long-range projections. *PLoS One* 7: e33537.
32. Signoretti S, Vagnozzi R, Tavazzi B, Lazzarino G (2010) Biochemical and neurochemical sequelae following mild traumatic brain injury: summary of experimental data and clinical implications. *Neurosurg Focus* 29: E1.
33. van der Stelt M, Di Marzo V (2005) Cannabinoid receptors and their role in neuroprotection. *Neuromolecular Med* 7: 37–50.
34. Milton NG (2002) Anandamide and noladin ether prevent neurotoxicity of the human amyloid-beta peptide. *Neurosci Lett* 332: 127–130.
35. Marsicano G, Moosmann B, Hermann H, Lutz B, Behl C (2002) Neuroprotective properties of cannabinoids against oxidative stress: role of the cannabinoid receptor CB1. *J Neurochem* 80: 448–456.
36. Kristensen BW, Norberg J, Zimmer J (2001) Comparison of excitotoxic profiles of ATPA, AMPA, KA and NMDA in organotypic hippocampal slice cultures. *Brain Res* 917: 21–44.
37. Ludanyi A, Hu SS, Yamazaki M, Tanimura A, Piomelli D, et al. (2011) Complementary synaptic distribution of enzymes responsible for synthesis and inactivation of the endocannabinoid 2-arachidonoylglycerol in the human hippocampus. *Neuroscience* 174: 50–63.
38. Uchigashima M, Yamazaki M, Yamasaki M, Tanimura A, Sakimura K, et al. (2011) Molecular and morphological configuration for 2-arachidonoylglycerol-mediated retrograde signaling at mossy cell-granule cell synapses in the dentate gyrus. *J Neurosci* 31: 7700–7714.
39. Katona I, Urban GM, Wallace M, Ledent C, Jung KM, et al. (2006) Molecular composition of the endocannabinoid system at glutamatergic synapses. *J Neurosci* 26: 5628–5637.
40. Stella N, Schweitzer P, Piomelli D (1997) A second endogenous cannabinoid that modulates long-term potentiation. *Nature* 388: 773–778.
41. Pan B, Wang W, Zhong P, Blankman JL, Cravatt BF, et al. (2011) Alterations of endocannabinoid signaling, synaptic plasticity, learning, and memory in monoacylglycerol lipase knock-out mice. *J Neurosci* 31: 13420–13430.
42. Straiker A, Wager-Miller J, Hu SS, Blankman JL, Cravatt BF, et al. (2011) COX-2 and fatty acid amide hydrolase can regulate the time course of depolarization-induced suppression of excitation. *Br J Pharmacol* 164: 1672–1683.
43. Gao Y, Vasilyev DV, Goncalves MB, Howell FV, Hobbs C, et al. (2010) Loss of retrograde endocannabinoid signaling and reduced adult neurogenesis in diacylglycerol lipase knock-out mice. *J Neurosci* 30: 2017–2024.
44. Goncalves MB, Suetterlin P, Yip P, Molina-Holgado F, Walker DJ, et al. (2008) A diacylglycerol lipase-CB2 cannabinoid pathway regulates adult subventricular zone neurogenesis in an age-dependent manner. *Mol Cell Neurosci* 38: 526–536.
45. Garcia-Ovejero D, Arevalo-Martin A, Petrosino S, Docagne F, Hagen C, et al. (2009) The endocannabinoid system is modulated in response to spinal cord injury in rats. *Neurobiol Dis* 33: 57–71.
46. Yazaki M, Kashiwagi K, Aritake K, Urade Y, Fujimori K (2012) Rapid degradation of cyclooxygenase-1 and hematopoietic prostaglandin D synthase through ubiquitin-proteasome system in response to intracellular calcium level. *Mol Biol Cell* 23: 12–21.
47. Yin H, Gui Y, Du G, Frohman MA, Zheng XL (2010) Dependence of phospholipase D1 multi-monoubiquitination on its enzymatic activity and palmitoylation. *J Biol Chem* 285: 13580–13588.
48. Clague MJ, Urbe S (2010) Ubiquitin: same molecule, different degradation pathways. *Cell* 143: 682–685.
49. Wickliffe K, Williamson A, Jin L, Rape M (2009) The multiple layers of ubiquitin-dependent cell cycle control. *Chem Rev* 109: 1537–1548.
50. Yoshida T, Fukaya M, Uchigashima M, Miura E, Kamiya H, et al. (2006) Localization of diacylglycerol lipase- α around postsynaptic spine suggests close proximity between production site of an endocannabinoid, 2-arachidonoylglycerol, and presynaptic cannabinoid CB1 receptor. *J Neurosci* 26: 4740–4751.
51. Uchigashima M, Narushima M, Fukaya M, Katona I, Kano M, et al. (2007) Subcellular arrangement of molecules for 2-arachidonoyl-glycerol-mediated retrograde signaling and its physiological contribution to synaptic modulation in the striatum. *J Neurosci* 27: 3663–3676.
52. Gomez O, Arevalo-Martin A, Garcia-Ovejero D, Ortega-Gutierrez S, Cisneros JA, et al. (2010) The constitutive production of the endocannabinoid 2-arachidonoylglycerol participates in oligodendrocyte differentiation. *Glia* 58: 1913–1927.
53. Walter L, Dinh T, Stella N (2004) ATP induces a rapid and pronounced increase in 2-arachidonoylglycerol production by astrocytes, a response limited by monoacylglycerol lipase. *J Neurosci* 24: 8068–8074.
54. Walter L, Franklin A, Witting A, Wade C, Xie Y, et al. (2003) Nonpsychotropic cannabinoid receptors regulate microglial cell migration. *J Neurosci* 23: 1398–1405.
55. Witting A, Chen L, Cudaback E, Straiker A, Walter L, et al. (2006) Experimental autoimmune encephalomyelitis disrupts endocannabinoid-mediated neuroprotection. *Proc Natl Acad Sci U S A* 103: 6362–6367.
56. Stella N (2004) Cannabinoid signaling in glial cells. *Glia* 48: 267–277.
57. Fernandez-Ruiz J, Pazos MR, Garcia-Arencibia M, Sagredo O, Ramos JA (2008) Role of CB2 receptors in neuroprotective effects of cannabinoids. *Mol Cell Endocrinol* 286: S91–96.
58. Savinainen JR, Saario SM, Laitinen JT (2012) The serine hydrolases MAGL, ABHD6 and ABHD12 as guardians of 2-arachidonoylglycerol signalling through cannabinoid receptors. *Acta Physiol (Oxf)* 204: 267–276.
59. Fiskerstrand T, H'Mida-Ben Brahim D, Johansson S, M'Zahem A, Haukanes BL, et al. (2010) Mutations in ABHD12 cause the neurodegenerative disease PHARC: An inborn error of endocannabinoid metabolism. *Am J Hum Genet* 87: 410–417.
60. McPartland JM, Norris RW, Kilpatrick CW (2007) Coevolution between cannabinoid receptors and endocannabinoid ligands. *Gene* 397: 126–135.
61. Schlosburg JE, Blankman JL, Long JZ, Nomura DK, Pan B, et al. (2010) Chronic monoacylglycerol lipase blockade causes functional antagonism of the endocannabinoid system. *Nat Neurosci* 13: 1113–1119.
62. Chanda PK, Gao Y, Mark L, Btresh J, Strassle BW, et al. (2010) Monoacylglycerol lipase activity is a critical modulator of the tone and integrity of the endocannabinoid system. *Mol Pharmacol* 78: 996–1003.
63. Zhao Y, Yuan Z, Liu Y, Xue J, Tian Y, et al. (2010) Activation of cannabinoid CB2 receptor ameliorates atherosclerosis associated with suppression of adhesion molecules. *J Cardiovasc Pharmacol* 55: 292–298.
64. Degn M, Lambertsen KL, Petersen G, Meldgaard M, Artmann A, et al. (2007) Changes in brain levels of N-acyl ethanolamines and 2-arachidonoylglycerol in focal cerebral ischemia in mice. *J Neurochem* 103: 1907–1916.
65. Panikashvili D, Shein NA, Mechoulam R, Trembovler V, Kohen R, et al. (2006) The endocannabinoid 2-AG protects the blood-brain barrier after closed head injury and inhibits mRNA expression of proinflammatory cytokines. *Neurobiol Dis* 22: 257–264.